The stretching vibrational overtone spectra of PH_3: Local mode vibrational analysis, dipole moment surfaces from density functional theory and band intensities

Sheng-Gui He,[a] Jing-Jing Zheng, Shui-Ming Hu, Hai Lin,[b] Yun Ding, Xiang-Huai Wang, and Qing-Shi Zhu
Open Laboratory of Bond Selective Chemistry, and the Institute for Advanced Studies, University of Science and Technology of China, Hefei, 230026, People's Republic of China

(Received 3 November 2000; accepted 9 January 2001)

The infrared spectra of PH_3 molecule were recorded on a Bruker IFS 120HR Fourier transform spectrometer from 4000 to 9500 cm^{-1}. The P–H stretching vibrational frequencies and intensities were derived from the experimental data. The Morse oscillator parameters D_e and α in the anharmonically coupled anharmonic oscillator local mode model were determined by the least-squares fitting with the observed vibrational band centers. The *ab initio* three-dimensional P–H stretching dipole moment surfaces were calculated by the density functional theory method. The dipole moment vectors were projected to three kinds of molecule-fixed reference systems. The corresponding dipole moment components were fitted to polynomial functions in terms of the P–H bond length displacements with the molecular symmetry taken into account. The absolute band intensities were obtained and then compared with the experimental data. The results showed that a proposed improved bond dipole model can predict the absolute band intensities within a factor of 2 for most of the observed transitions, indicating a reasonably good agreement. © *2001 American Institute of Physics.* [DOI: 10.1063/1.1352038]

I. INTRODUCTION

The phosphine molecule is a subject of considerable spectroscopic and astronomical interest. Its infrared spectrum is characterized by significant Coriolis and Fermi resonances.[1] The A_1-A_2 splittings in the v_2 symmetric and v_4 antisymmetric bending fundamentals have been intensively studied.[2,3] Similar to AsH_3 and SbH_3 molecules, the near degenerate v_1 symmetric and v_3 antisymmetric stretching modes have also drawn some attention to the local mode study.[4] Additionally, PH_3 is important for the studies of the atmosphere of Jupiter and Saturn[5,6] where it has already been observed.[7]

The present work mainly contributes to the P–H stretching vibrational band intensities. The local mode notation $(n_1n_2n_3;\Gamma)$[8] will be adopted to identify the vibrational states. The fundamentals $(100;A_1)$ and $(100;E)$ were studied by McKean and Schatz[9] and Baldacci, Devi, and Rao.[10] The stretching overtone spectra up to $V=3$ were recorded by Wang and Zhu,[4] here $V=n_1+n_2+n_3$, but the band intensities cannot be found in their work. In this work, we re-record the high-resolution Fourier transform infrared (FTIR) spectra up to $V=4$ and report the band intensities and some new band centers.

Theoretical calculations on the local mode vibrational intensities of various XH(X=C, N, O, Si, P, As, and so on) bond oscillators can be mainly divided into two sorts. The first type of studies[11–13] is based on the bond dipole model,[8,14,15] where the molecule dipole moment vector is assumed to be a sum of the individual bond dipole moment vectors along the bond directions

$$\boldsymbol{M}=\sum_{i=1}^{n} M_i\mathbf{e}_i . \tag{1}$$

Here, M_i is the bond dipole function which only depends on the ith bond length and $\mathbf{e}_i$ is the unit vector along this bond. Various bond dipole functions have been proposed to model the bond dipole moment. The Mecke-type function[16] is widely applied because it possesses correct asymptotic behavior as the bond length approaches infinity. The Mecke-type function contains three empirical parameters which are adjusted either to fit the *ab initio* dipole moment data points,[17,18] or to make the calculated intensities close to the observed values.[13,19] Though it generally gives qualitative agreement between calculations and observations, it fails in some cases due to the neglecting of the inter-bond coupling contribution. For local mode molecules and with the bond dipole model, the overtone band intensity will be more intense than that of the combination band.[8] However, in some cases, the intensity anomaly was found in the experiment, for example, the overtone band $(4000;A_1/F_2)$ is weaker than the combination $(3100;A_1/F_2)$ in germane,[20] and $(3000;A_1/F_2)$ is weaker than $(2100;A_1/F_2)$ in silane.[21] Similar phenomena have also been found in neopentane,[22] propane,[23] dimethyl ether,[24] and hydrogen peroxide.[25] The intensity anomaly in PH_3 was also found in our measurement. So, it means the empirical bond dipole model must be

[a]Author to whom correspondence should be addressed; electronic mail: hsg@mail.ustc.edu.cn
[b]Current address: Anorganische Chemie, Fachbereich 9, Universität-Gesamthochschule Wuppertal, D-42097 Wuppertal, Germany.

improved in order to depict the intensity anomaly, although it is so simple and has some physical intuition.

Studies of the second type are not based on the bond dipole model. Henry, Kjaergaard, and their co-workers used dipole moment functions which were expressed as a series expansion in terms of internal X–H stretching coordinates to study the X–H bond oscillator intensities in H_2O, H_2O_2, NH_3, HCN, CH_2O, CHD_2F, CH_4, C_6H_6, and so on,[26–28] and very recently in $C_6H_5CH_3$.[29] Another example is the O–H stretching overtone intensities of the HOD molecule investigated by Fair, Votava, and Nesbitt.[30] They found that the observation was in excellent agreement with full three-dimensional (3D) quantum variational calculations based on the H_2O potential surface by Polyansky, Jensen, and Tennyson[31] and dipole moment surface by Gabriel *et al.*[32] The bond dipole model was, however, found to be not so successful in these cases.

In this article, we use the *ab initio* calculated dipole moment surfaces (DMSs) to predict the absolute band intensities of PH_3 and try to depict the intensity anomaly since the *ab initio* DMSs successfully produced the relative and absolute band intensities of C–H chromophore in $CHCl_3$, $CHBr_3$, and CHI_3 in our earlier work.[33,34] The outline of the remainder of this article is as follows. In Sec. II, the experimental details are given. In Sec. III, we report the 3D P–H stretching DMSs by the density functional theory (DFT) method. The dipole moment vectors are projected to three kinds of reference systems, they are (1) the one which obeys Eckart conditions,[35,36] (2) the one in which the axis directions are along the principal inertial axes in the equilibrium configuration, and (3) the one in which the axes are along three P–H bonds. Different dipole moment models are used to fit the corresponding *ab initio* calculated dipole moment components. In Sec. IV, the absolute band intensities are calculated and then compared with experimental data. The results are given and discussed in Sec. V, and conclusions are drawn in Sec. VI.

II. EXPERIMENT

A. Sample and instrument configurations

The PH_3 sample was purchased from Nanjing Special Gas Company with a stated purity of 99.99%. The high-resolution spectra of PH_3 from $V=2$ through $V=4$ were recorded by utilizing a Bruker IFS 120HR Fourier transform spectrometer which was equipped with a path length adjustable multi-pass gas cell. A tungsten source and a CaF_2–Si beamsplitter were used for all the spectra. A liquid nitrogen cooled HgCdTe detector and an IR bandpass filter whose cutoff frequencies are 4050 and 5000 cm^{-1} were used to obtain the $V=2$ spectrum at an unapodized resolution of 0.01 cm^{-1}, while the $V=3$ and 4 spectra were obtained using an InGaAs detector with resolutions of 0.015 and 0.02 cm^{-1}, respectively. The sample pressures and absorptional path lengths were 307 Pa, 15 m; 3623 Pa, 87 m and 8960 Pa, 105 m for $V=2$, 3, and 4, respectively. The pressures were measured by a manometer with an absolute pressure accuracy of 50 Pa. All the spectra were observed at room temperature which varied from 19.8 to 21.8 °C in the measurement.

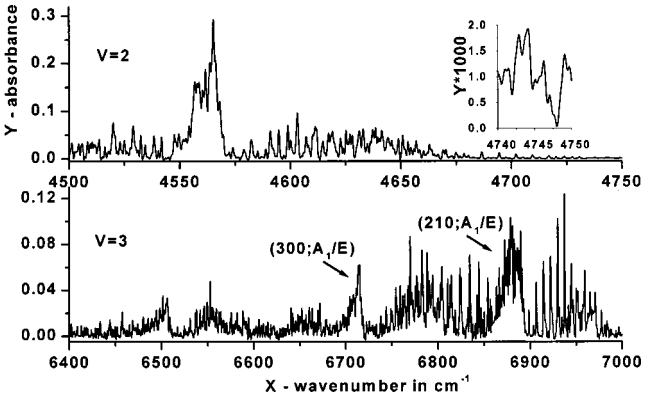

FIG. 1. FTIR spectra of PH_3 molecule in $V=2$ (upper panel) and 3 (lower) regions. The unapodized resolution is 0.5 cm^{-1}. The sample pressures and absorptional path lengths are 307 Pa, 15 m, and 3623 Pa, 87 m for $V=2$ and 3, respectively.

B. Analysis

Since the present work is focused on the stretching vibrational band intensities, only a portion of the interferogram of the high-resolution spectrum is used to do the Fourier transform to get the medium-resolution spectrum with higher signal-to-noise ratios (SNRs). All the resolutions are set to 0.5 cm^{-1}, and the SNRs are all better than 2500 for the spectrum base lines. The $V=2$ and 3 spectra are illustrated in Fig. 1. In the upper panel of the figure, the strong absorptions centered at 4566 cm^{-1} are assigned to the $(200;A_1/E)$ bands, and a clearly R branch of a weak parallel band assigned to $(110;A_1)$[4] is located in the high frequency side. The $V=3$ and 4 spectra are more complicated due to strong rovibrational interactions, for example, in the $V=3$ spectrum shown in the lower panel of Fig. 1, the bands centered at 6715 cm^{-1} are assigned to $(300;A_1/E)$ and the more intense absorptions located at 6885 cm^{-1} are $(210;A_1/E)$ bands; the intensity anomaly is clearly shown. Some roughly rovibrational analysis based on the Hamiltonian model in Ref. 3 has been carried out on the high-resolution spectra of $V=2$ and 3 to get more confident band centers; the results with those of the earlier work are listed in Table I. Some bands associated with the bending motions are also observed in the measurement. They are listed in Table II; further vibrational analysis considering the bending modes will be discussed elsewhere. The band intensities are obtained by directly integrating of the absorbance spectra

$$I(v_0)=\int_{v_0-v_L}^{v_0+v_H}-\ln[S(v)/S_0(v)]dv, \tag{2}$$

where, v_0 is the band center, v_L and v_H are the appropriate values for the integral limits, and $S(v)$ and $S_0(v)$ are the transmittance and base line spectra, respectively. The intensities with v_L and v_H are listed in Table I. The absolute intensity uncertainties will be discussed in the following paragraph.

TABLE I. Observed stretching vibrational band centers and intensities of PH_3 molecule.

$(n_1n_2n_3;\Gamma)$	v_0 cm^{-1}	I_{exp}[a] cm^{-1}	v_L/v_H cm^{-1}	$I_{obs.}$[b] 10^{-22} cm	Δ_{Tot} %
$(100;A_1)$[c]	2321.1314			45800	
$(100;E)$[c]	2326.8766			163000	
$(200;A_1)$	4566.26[d]	6.77	150/188	567[e]	21
$(200;E)$	4565.78[d]				
$(110;A_1)$	4644.66[d]			29.8[f]	30–40
$(300;A_1/E)$	6714.60[d]	2.54	81.6/83.4	3.27	21
$(210;A_1)$[g]	6881.533	3.93	83.5/128.5	4.71[h]	22
$(210;lE)$[g]	6883.731				
$(210;hE)$[g]	6890.861				
$(111;A_1)$[i]	6971.1576	0.274		0.353	18
$(400;A_1/E)$	8788.0	1.86	188/118	0.802	22
$(310;A_1/E)$	9040.0	0.94	134/110	0.406	24

[a]Obtained with Eq. (2) in the text.
[b]$I_{obs.}=I_{exp.}\,kT/P/L$; here k, P, L, and T are the *Boltzmann* constant, sample pressure, absorptional path length, and temperature in the measurement, respectively. $T=294$ K is used in the calculation.
[c]References 9 and 10.
[d]Reference 4.
[e]Total intensity of $(200;A_1)$ and $(200;E)$.
[f]Estimated from the peak height of the strong lines of the R branch in the high-resolution spectrum.
[g]Three strong coupled vibrational bands by Coriolis resonance.
[h]Total intensity of $(210;A_1)$, $(210;lE)$, and $(210;hE)$.
[i]An unperturbed weak transition with a typical K structure of the parallel band. The intensity is obtained by integrating all the assigned lines of $(111;A_1)$ band in the high-resolution spectrum.

The intensity uncertainties originate from the following five reasons. (1) The low SNR, which is especially critical for weak absorptions; this uncertainty can be estimated as $\Delta_{SNR}=(v_L+v_H)/SNR$. Table I shows the largest relative intensity uncertainty for $(310;A_1/E)$ is about $0.1/0.94=11\%$, here SNR=2500 is used. (2) The nonlinear response of the instruments (for example, the detector) to the light intensity at a specific frequency, by comparing the H_2O absorption in the high-resolution spectra with the intensities listed in the HITRAN 96 database;[37] we estimate this uncertainty to be 10%. (3) The molecule density uncertainty which comes from the pressure, temperature, and the absorptional path length uncertainties; the last two which lead to less than 1% uncertainty can be neglected. As to the sample pressure, the relative uncertainty for $V=3$ and 4 can also be neglected, for $V=2$ it is about 15%. (4) The band overlapping, in Fig. 1, the P branch of $(300;A_1/E)$ overtones is overlapped with $2v_1+2v_2{}^4$ centered at 6503 cm^{-1} and the R branch overlapped with P branch of $(210;A_1/E)$. In this case, the v_L and v_H in Eq. (2) are chosen such that the integral limit is just in the middle of the two neighboring band centers. Because the different band intensities in $V=3$ are comparable and the band centers are well isolated, this method is reasonable and the uncertainty is estimated to be 15% for $V=3$ spectrum. Another one is the overlapping with H_2O absorption, which is critical for $V=4$ spectrum. The H_2O contribution to the intensity is deleted by calibrating the H_2O lines in the high-resolution spectra with the ones listed in the HITRAN 96 database,[37] the corresponding uncertainties are estimated to be 15% for $V=4$ spectrum and 5% for $(210;A_1/E)$ bands of which a portion of the R branch is overlapped with H_2O lines. (5) The base line uncertainty, the PH_3 lines are condensed and we obtain the base line spectrum $S_0(v)$ from the area between the lines in the transmittance spectrum $S(v)$, so it also leads to the intensity uncertainty, which is estimated to be 10%. It can be seen that the main intensity uncertainties come from the pressure uncertainty for $V=2$, and the band overlapping for $V=3$ and 4. The total uncertainties can be estimated as $\Delta_{Tot}=\sqrt{\Delta_1^2+\Delta_2^2+\Delta_3^2+\Delta_4^2+\Delta_5^2}$, which are also listed in Table I; here Δ_i is the ith relative uncertainty mentioned above.

TABLE II. Observed band centers (cm^{-1}) associated with the bending modes of PH_3 molecule.

v_0	$(n_1n_2n_3;v_2v_4^{l_4};\Gamma)$[a]	ν_0	$(n_1n_2n_3;v_2v_4^{l_4};\Gamma)$[a]
992.134 767	$(000;10^0;A_1)$[b]	3896.023	$(000;40^0;A_1)$[d]
1118.306 385	$(000;01^{\pm1};E)$[b]	4282.4	$(100;20^0;A_1)$[e]
1972.5454	$(000;20^0;A_1)$[c]	5540.0	$(200;10^0;\Gamma)$[f]
2108.0458	$(000;11^{\pm1};E)$[c]	5645.4	$(200;01^{\pm1};\Gamma)$[f]
2940.772	$(000;30^0;A_1)$[d]	6503.1	$(200;20^0;A_1)$[e]
3214.2	$(000;12^0;A_1)$[e]	7679.1	$(300;10^0;\Gamma)$[f]
3305.8	$(100;10^0;A_1)$[e]	7775.5	$(300;01^{\pm1};\Gamma)$[f]
3423.9	$(100;01^{\pm1};\Gamma)$[f]	7961.9	$(210;01^{\pm1};\Gamma)$[f](?)

[a]Assignment, normal mode notation is used for the bending modes.
[b]Reference 3.
[c]Reference 50.
[d]Reference 51.
[e]Reference 4.
[f]This work.

III. DIPOLE MOMENT SURFACES AND DIPOLE MOMENT MODELS

The procedure to calculate the 3D stretching DMSs of PH_3 by the DFT method is similar to the one used for trihalomethanes in our earlier work.[33,34] Briefly, it involves two steps: (1) geometry optimization and (2) single point calculations which give the data points on the DMSs. In both steps, the B3LYP (Becke's three parameter hybrid method with the correlation functional of Lee, Yang, and Parr, which includes both local and nonlocal terms)[38] method with the 6-311++G(3df,2pd) basis set[39] are used. The calculations are performed by using the GAUSSIAN 94 package.[40] The optimized geometry with those obtained from experiments are listed in Table III; the dipole moment at this configuration and the ground state dipole transition moment from experiment are also listed. It is shown that the agreements are good. When evaluating the dipole moment, only the three P–H bonds are stretched while the three H–P–H bond angles are kept to their equilibrium values. In the calculation, each bond length displacement $r_i(i=1,2,3)$ varies from -0.3 Å to 0.4 Å by the step of 0.05 Å, Considering the C_{3v} point group symmetry of the molecule, we only calculate the data points at the configurations of $r_1 \geqslant r_2 \geqslant r_3$ to get 680 *ab initio* data points since the dipole moments at other configurations can be easily derived.[34]

The calculated *ab initio* dipole moment vectors are projected to three sets of molecule-fixed reference systems which are denoted to be R_{Prin}, R_{Eck}, and R_{Bond}. In R_{Bond}, the dipole moment vector $\mathbf{M}$ is projected as

TABLE III. Comparison of the optimized and experimental equilibrium geometric structure and permanent dipole moment of PH_3 molecule.

	This work	Expt. 1[a]	Expt. 2[b]	Expt. 3[c]	Expt. 4[d]
R_{PH} (Å)	1.4179	1.412 03(70)	1.411 75(50)	1.411 59(60)	⋯
ϕ_{HPH} (°)	93.4318	93.407(40)	93.421(60)	93.328(20)	⋯
u_0 (Debye)	0.5763	⋯	⋯	⋯	0.573 95(30)

[a]Reference 4.
[b]Reference 52.
[c]Reference 53.
[d]Reference 54.

$$\mathbf{M}(r_1,r_2,r_3)=u_1(r_1,r_2,r_3)\mathbf{e}_1+u_2(r_1,r_2,r_3)\mathbf{e}_2+u_3(r_1,r_2,r_3)\mathbf{e}_3, \tag{3}$$

where $\mathbf{e}_i(i=1,2,3)$ is the unit vector along the P–H_i bond, and H_i is the ith H atom in PH_3. In this work, we let $\mathbf{e}_1$, $\mathbf{e}_2$, and $\mathbf{e}_3$ be left handed, i.e., $(\mathbf{e}_1\times\mathbf{e}_2)\cdot\mathbf{e}_3<0$. It can be seen that R_{Bond} is not a right-angled reference system. The three unit vectors along the right-angled axes of x, y, and z in R_{Prin} are defined as

$$\mathbf{e}_z=-(\mathbf{e}_1+\mathbf{e}_2+\mathbf{e}_3)/|(\mathbf{e}_1+\mathbf{e}_2+\mathbf{e}_3)|, \tag{4}$$

$$\mathbf{e}_y=\mathbf{e}_z\times\mathbf{e}_1/|\mathbf{e}_z\times\mathbf{e}_1|, \tag{5}$$

$$\mathbf{e}_x=\mathbf{e}_y\times\mathbf{e}_z, \tag{6}$$

and the dipole moment vector $\mathbf{M}$ is

$$\mathbf{M}(r_1,r_2,r_3)=u_x(r_1,r_2,r_3)\mathbf{e}_x+u_y(r_1,r_2,r_3)\mathbf{e}_y+u_z(r_1,r_2,r_3)\mathbf{e}_z. \tag{7}$$

It is clear that x, y and z are the principal inertial axes in the equilibrium configuration. In order to get the result with the best separation of vibrational and rotational motion,[41] the reference system which obeys Eckart conditions[35,36] is also used; it is denoted as R_{Eck}. A simple Fortran code which is based on the multidimensional conjugate gradient method[42] has been written to solve the Eckart conditions. It is shown that the three right-angled axes of ξ, η, and ζ in R_{Eck} are almost superposed with x, y, and z in R_{Prin}. The maximal Euler angle[36] is only 0.01 radian at the configuration of $(r_1,r_2,r_3)=(-0.3,0.4,0.4)$ Å, which shows R_{Prin} and R_{Bond} are also the reference systems with good separation of the vibrational and rotational motion.

Similar to our earlier work,[33,34] the polynomial functions in terms of the bond length displacements are also used here to expand the DMSs. The PH_3 molecule has the symmetry of point group C_{3v}, so we have the following relations for u_1, u_2, and u_3:

$$u_2(r_1,r_2,r_3)=u_1(r_2,r_1,r_3), \tag{8}$$

$$u_3(r_1,r_2,r_3)=u_1(r_3,r_2,r_1) \tag{9}$$

and

$$u_1(r_1,r_2,r_3)\equiv u(r_1,r_2,r_3)=f(r_1)[g(r_2,r_3)+g(r_3,r_2)], \tag{10}$$

where $f(x)$ and $g(x,y)$ are any functions. The $u(r_1,r_2,r_3)$ is expanded as

$$u(r_1,r_2,r_3)=\sum_{i,j\geqslant k} C^B_{ijk}r_1^i(r_2^jr_3^k+r_2^kr_3^j)/(1+\delta_{jk}), \tag{11}$$

where i, j, and k are non-negative integers, C^B_{ijk} is the expansion coefficient, and $\delta_{jk}=1$ if $j=k$, or else $\delta_{jk}=0$.

As to the three components of the DMSs in R_{Prin}, u_x, u_y, and u_z have the E_x, E_y, and A_1 representations of the C_{3v} point group, respectively, so we should use the corresponding polynomial functions in terms of symmetric internal coordinates to expand them. Up to third order, the u_x, u_y and u_z are

$$u_x(r_1,r_2,r_3)=C^x_{100}E^x_{100}+C^x_{200}E^x_{200}+C^x_{110}E^x_{110}+C^x_{300}E^x_{300}+C^{x1}_{210}E^{x1}_{210}+C^{x2}_{210}E^{x2}_{210}, \tag{12}$$

$$u_y(r_1,r_2,r_3)=C^y_{100}E^y_{100}+C^y_{200}E^y_{200}+C^y_{110}E^y_{110}+C^y_{300}E^y_{300}+C^{y1}_{210}E^{y1}_{210}+C^{y2}_{210}E^{y2}_{210}, \tag{13}$$

$$u_z(r_1,r_2,r_3)=C^z_{000}+C^z_{100}S_{100}+C^z_{200}S_{200}+C^z_{110}S_{110}+C^z_{300}S_{300}+C^z_{210}S_{210}+C^z_{111}S_{111}, \tag{14}$$

where $C^\alpha_{ijk}(\alpha=x,y,z,x1,x2,y1,y2)$ is the expansion coefficient, E^α_{ijk} and S_{ijk} are the following:

$$E^x_{ijj}=(r_1r_2r_3)^j(2r_1^{i-j}-r_2^{i-j}-r_3^{i-j})/\sqrt{6}, \tag{15}$$

$$E^x_{iij}=(r_1r_2r_3)^i(2r_1^{j-i}-r_2^{j-i}-r_3^{j-i})/\sqrt{6}, \tag{16}$$

$$E^{x1}_{ijk}=[2r_1^i(r_2^jr_3^k+r_2^kr_3^j)-r_1^j(r_2^ir_3^k+r_2^kr_3^i)-r_1^k(r_2^ir_3^j+r_2^jr_3^i)]/\sqrt{12}, \tag{17}$$

$$E^{x2}_{ijk}=[r_1^k(r_2^ir_3^j+r_2^jr_3^i)-r_1^j(r_2^ir_3^k+r_2^kr_3^i)]/2, \tag{18}$$

$$E^y_{ijj}=(r_1r_2r_3)^j(r_2^{i-j}-r_3^{i-j})/\sqrt{2}, \tag{19}$$

$$E^y_{iij}=(r_1r_2r_3)^i(r_2^{j-i}-r_3^{j-i})/\sqrt{2}, \tag{20}$$

$$E^{y1}_{ijk}=[r_1^k(r_2^ir_3^j-r_2^jr_3^i)+r_1^j(r_2^ir_3^k-r_2^kr_3^i)]/2, \tag{21}$$

$$E^{y2}_{ijk}=[2r_1^i(r_2^jr_3^k-r_2^kr_3^j)+r_1^j(r_2^ir_3^k-r_2^kr_3^i)+r_1^k(r_2^jr_3^i-r_2^ir_3^j)]/\sqrt{12}, \tag{22}$$

$$S_{iii}=(r_1r_2r_3)^i, \tag{23}$$

$$S_{ijj}=(r_1r_2r_3)^j(r_1^{i-j}+r_2^{i-j}+r_3^{i-j})/\sqrt{3}, \tag{24}$$

$$S_{iij}=(r_1r_2r_3)^i(r_1^{j-i}+r_2^{j-i}+r_3^{j-i})/\sqrt{3}, \tag{25}$$

TABLE IV. Expansion coefficients[a] of the dipole moment surfaces of PH_3 molecule with different dipole moment models (DMMs).

	DMM_1		DMM_2	DMM_3
C^B_{000}	0.354 181(98)	$C^{z\,b}_{000}$	−0.574 91(14)	−0.574 95(14)
C^B_{100}	−1.078 27(59)	C^z_{100}	0.912 67(74)	0.912 65(74)
C^B_{010}	0.048 95(34)	C^z_{200}	0.430 7(19)	0.406 9(19)
C^B_{200}	−0.585 6(14)	C^z_{110}	0.145 8(16)	0.170 0(16)
C^B_{020}	0.055 5(11)	C^z_{300}	−0.108 1(73)	−0.112 9(77)
C^B_{110}	−0.053 0(12)	C^z_{210}	−0.303 0(64)	−0.300 1(64)
C^B_{011}	−0.048 13(98)	C^z_{111}	0.065 2(60)	0.066 3(59)
C^B_{300}	0.222 5(59)	C^y_{100}	−1.165 44(84)	−1.154 71(85)
C^B_{030}	0[c]	C^y_{200}	−0.669 8(20)	−0.683 5(20)
C^B_{210}	0.039 8(50)	C^y_{110}	0.005 0(16)	0.014 1(16)
C^B_{021}	0[c]	C^y_{300}	0.294 4(83)	0.295 3(83)
C^B_{120}	0.182 3(50)	C^{y1}_{210}	−0.074 8(69)	−0.068 6(69)
C^B_{111}	−0.040 0(42)	C^{y2}_{210}	0.229 9(68)	0.224 1(68)
rms[d] ($\times 10^{-3}$)	2.91		2.87/2.80[e]	2.84/2.81[f]

[a]Units are defined such that the dipole moment is in Debye ($=3.335\,64\times10^{-30}$ C m), the bond length displacement in Å. The value in the parentheses is one standard error in the last significant digit. For DMM_1, u_2 and u_3 are obtained with Eqs. (8) and (9), while x and ξ components in DMM_2 and DMM_3 with Eq. (27).
[b]For DMM_3, using η and ς instead of y and z.
[c]Constrained value.
[d]Root mean squares of the fitting residual.
[e]For z and y components, respectively.
[f]For ς and η components, respectively.

$$S_{ijk}=[r_1^i(r_2^jr_3^k+r_2^kr_3^j)+r_1^j(r_2^ir_3^k+r_2^kr_3^i)+r_1^k(r_2^jr_3^i+r_2^ir_3^j)]/\sqrt{6}. \tag{26}$$

In Eqs. (15)–(26), i, j, and k are integers, and $i>j>k\geqslant 0$. Here, the coefficients of x and y components of the DMSs also have simple relations similar to those for CHX_3 molecules[34]

$$C^x_{ijk}=C^y_{ijk},\quad C^{x1}_{ijk}=C^{y1}_{ijk},\quad C^{x2}_{ijk}=-C^{y2}_{ijk}. \tag{27}$$

The form of these symmetric terms can also be constructed by coupling the linear terms S_{100}, E^x_{100}, and E^y_{100} repeatedly with themselves with the help of the vector-coupling coefficients tabulated in Refs. 43, 44. Some further information about the relations for the DMSs expansion coefficients in axially symmetric molecules can be referred to Ref. 45.

The dipole moment model in Eqs. (12)–(14) has also been applied to the three components of the DMSs in $R_{\rm Eck}$; we denote the corresponding expansion coefficients to be C^α_{ijk}, here $\alpha=\xi,\xi_1,\xi_2,\eta,\eta_1,\eta_2$ and ζ. For convenience, we called the dipole moment model in Eq. (11), in Eqs. (12)–(14) with $R_{\rm Prin}$ and $R_{\rm Eck}$ to be DMM_1, DMM_2, and DMM_3, respectively. The expansion coefficients are fitted with the *ab initio* calculated data points. The results are listed in Table IV. In practical fitting, it is, however, not necessary to include many high order terms which cannot be determined well. All the terms higher than third order are constrained to zeros. The C^B_{021} and C^B_{030} in DMM_1 are also set to zeros for the same reason. For illustration, parts of the *ab initio* calculated dipole moment along $P–H_1$ bond are plotted in Fig. 2, where the corresponding results fitted by DMM_1 are also shown.

IV. INTENSITIES CALCULATION

The absolute vibrational band intensity I can be calculated as

$$I(v_0)=\frac{8\pi^3v_0}{3hcQ_v(T)}\left[1-\exp\left(-\frac{hcv_0}{kT}\right)\right]|\langle N|\mathbf{M}|0\rangle|^2. \tag{28}$$

Here $|0\rangle$ and $|N\rangle$ denote the vibrational ground and excited states, v_0 is the transition wave number, T is the sample temperature in the measurement, $Q_v(T)$ is the vibrational partition function at temperature T, c is the speed of light, k and h are *Boltzmann* and *Planck* constants, respectively. The

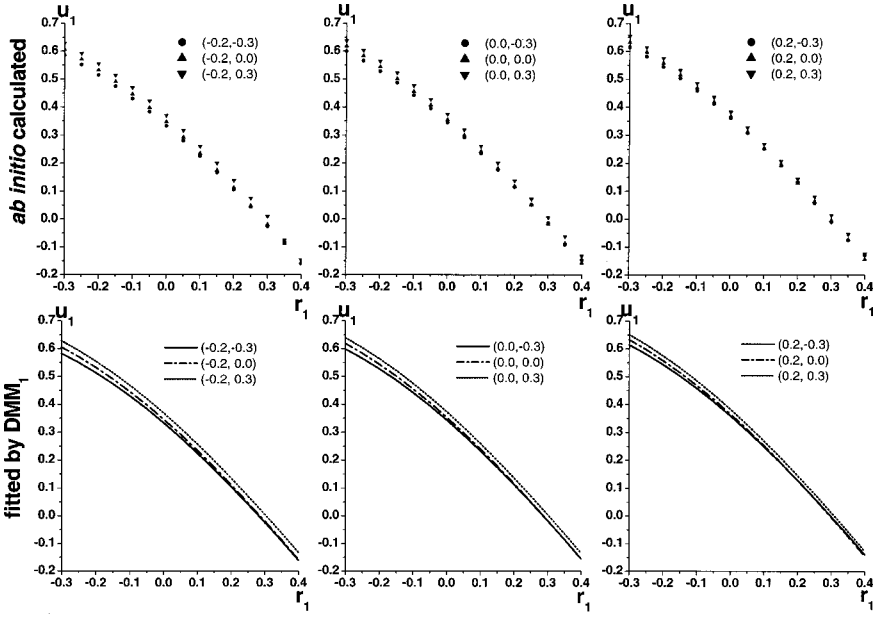

FIG. 2. The dipole moment along $P–H_1$ bond in PH_3 molecule varying with r_1 at different values of r_2 and r_3. Values in the parentheses are r_2 and r_3. Units are defined such that the dipole moment is in Debye ($=3.335\,64\times10^{-30}$ C m), the bond length displacement in Å. The upper panel is for the *ab initio* calculated dipole moment, and the corresponding result fitted by DMM_1 is in the lower panel.

TABLE V. Calculated band centers (in cm^{-1}) and intensities (in 10^{-22} cm) with ACAOI Hamiltonian and DMM_1, DMM_2, and DMM_3 dipole moment models. The observed intensities are also listed for comparison.

$(n_1n_2n_3;\Gamma)$	$v_{0\ calc.}$	I_{DMM_1}	I_{DMM_2}	I_{DMM_3}	$I_{obs.}$
$(100;A_1)$	2320.78	62 300/262 000[a]	61 600/262 000	61 500/260 000	45 800/209 000
$(100;E)$	2325.56	200 000	202 000	198 000	163 000
$(200;A_1)$	4561.91	222/637	219/637	250/615	/567
$(200;E)$	4562.30	415	418	365	
$(110;A_1)$	4645.06	21.6/21.6	21.7/21.7	30.3/30.5	/29.8
$(110;E)$	4649.68	0.005 72	0.006 05	0.215	
$(300;A_1)$	6714.85	0.244/5.85	0.080 8/9.60	0.302/12.1	/3.27
$(300;E)$	6714.88	5.61	9.52	11.8	
$(210;A_1)$	6881.62	3.94/6.39	4.18/6.65	4.69/9.96	/4.71
$(210;lE)$	6884.00	0.361	0.347	0.426	
$(210;hE)$	6888.95	2.09	2.12	2.02	
$(111;A_1)$	6972.49	0.114	0.116	0.124	0.353
$(400;A_1)$	8781.89	0.570/3.55	0.150/4.41	0.100/4.76	/0.802
$(400;E)$	8781.89	2.98	4.26	4.66	
$(310;A_1)$	9037.10	0.237/0.428	0.254/0.446	0.276/0.464	/0.406
$(310;lE)$	9037.60	0.0146	0.0159	0.0121	
$(310;hE)$	9040.51	0.176	0.176	0.176	
$(500;A_1)$	10 763.26	0.125/0.669	0.043 1/0.803	0.0350/0.847	
$(500;E)$	10 763.26	0.544	0.760	0.812	
$(600;A_1)$	12 658.97	0.0220/0.111	0.008 21/0.131	0.00706/0.137	
$(600;E)$	12 658.97	0.0886	0.123	0.130	
Δ_{log}[b]		0.311(0.715)	0.363(0.836)	0.382(0.880)	

[a]The value under / is the total intensity of the bands with the same quantum numbers $n_1n_2n_3$.
[b]Logarithmic deviation defined in Eq. (33) in the text, the value in the parentheses is in the natural logarithm.

spectra were recorded at room temperature and the lowest vibrational transition wave number of the PH_3 is 992 cm^{-1},[2] $[1-\exp(-hcv_0/kT)]\simeq 1$ and $Q_v(T)\simeq 1$ can be applied as good approximations. For dipole moment vector expressed as Eq. (3) in R_{Bond}, we have

$$I(v_0)=Kv_0[u_{1N}^2+u_{2N}^2+u_{3N}^2+2\cos(\phi) \times(u_{1N}u_{2N}+u_{1N}u_{3N}+u_{2N}u_{3N})], \quad (29)$$

while for R_{Prin} or R_{Eck} (use ξ, η, ζ instead of x, y, z), it is

$$I(v_0)=Kv_0(u_{xN}^2+u_{yN}^2+u_{zN}^2). \quad (30)$$

In Eqs. (29) and (30), $K=4.162\,3755\times10^{-19}\,cm^2\,Debye^{-2}$ (making use of $1\ Debye=3.335\,64\times10^{-30}\,C\,m$), $u_{iN}=\langle N|u_i|0\rangle$, here $i=1,2,3$, or x, y, z, and ϕ is the optimized H–P–H bond angle in Table III.

The vibrational wave functions are calculated variationally based on the anharmonically coupled anharmonic oscillator (ACAO) local mode model.[15,46] The stretching vibrational Hamiltonian is

$$H=\sum_{i=1}^{3}\left(\frac{1}{2}G_{rr}p_i^2+D_ey_i^2\right)+\sum_{i<j}^{3}(G_{rr'}p_ip_j+F_{rr'}r_ir_j), \quad (31)$$

or

$$H=\sum_{i=1}^{3}\left(\frac{1}{2}G_{rr}p_i^2+D_ey_i^2\right)+\sum_{i<j}^{3}\left(G_{rr'}p_ip_j+\frac{1}{\alpha^2}F_{rr'}y_iy_j\right), \quad (32)$$

where $y_i=1-\exp(-\alpha r_i)$, $G_{rr}=1/m_H+1/m_P$ (here m_H is the mass of the H atom and m_P the P atom), $G_{rr'}=\cos(\phi)/m_P$ and $\phi=93.407°$ is used in this work, p_i is the momentum conjugate to r_i, D_e and α are the Morse potential parameters, and $F_{rr'}$ is the inter-bond potential coupling parameter. The models in Eqs. (31) and (32) are called ACAOI and ACAOII, respectively. The method to construct the symmetric wave functions and the Hamiltonian matrice has been described elsewhere,[15,47] some further references about the elements of the momentum and position operators in the Morse functional basis can be found in Refs. 8 and 15. The D_e and α are optimized by the least-squares fitting with the observed vibrational band centers listed in Table I, while $F_{rr'}$ which cannot be determined well in the fitting is constrained to the recently *ab initio* calculated value by Wang *et al.* in Ref. 48, where the adjusted values of F_{11} and F_{33} are cited to calculate $F_{rr'}$. The results are $F_{rr'}=74.50\,cm^{-1}\,Å^{-2}$, $D_e=33\,890\,(125)\,cm^{-1}$ and $\alpha=1.574\,74(323)\,Å^{-1}$ for ACAOI, $D_e=33\,875(118)\,cm^{-1}$, and $\alpha=1.575\,19(307)\,Å^{-1}$ for ACAOII. The value in the parentheses is one standard error in the last significant digit. The maximal vibrational quantum number V_{max} is set to 12 in the optimization. The band centers of $(200;A_1/E)$, $(400A_1/E)$, and $(310;A_1/E)$ in Table I are found to be perturbed to the higher frequency side by about 3–6 cm^{-1}, which can be explained by the Fermi resonance with the bending modes from the lower frequency side. These band centers are discarded in the optimization and all others are unit weighted. The root mean squares (rms) of the fitting residual are 1.05 cm^{-1} for ACAOI and 0.99 cm^{-1} for ACAOII. The band intensities have been calculated accord-

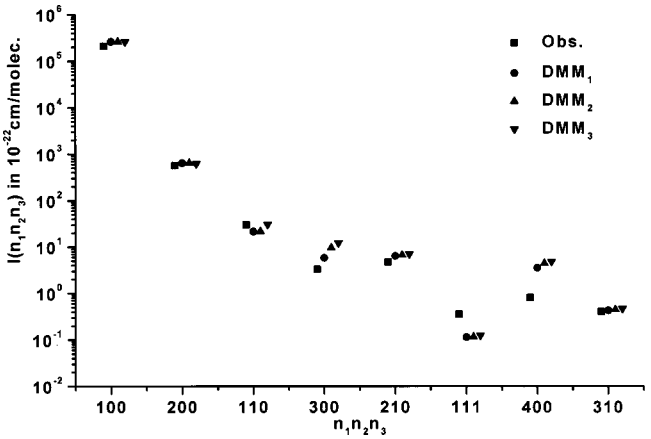

FIG. 3. Absolute band intensities of PH_3 molecule by observation and calculation with different dipole moment models (DMMs).

ing to Eqs. (29) and (30). The results by ACAOI with the DMM_1, DMM_2, and DMM_3 are listed in Table V, while those by ACAOII which are almost the same have been omitted.

V. RESULTS AND DISCUSSIONS

It can be seen from Table V that the predictions agree with the observations reasonably well. Logarithmic deviation[12] is defined to yield the estimation of the agreement

$$\Delta_{\log}^2=\frac{1}{n_{\text{data}}}\sum_{n_1n_2n_3}^{n_{\text{data}}}\left[\log_{10}\frac{I_{\text{calc.}}(n_1n_2n_3)}{I_{\text{obs.}}(n_1n_2n_3)}\right]^2, \tag{33}$$

where n_{data} is the number of the experimental data points, $I_{\text{calc.}}(n_1n_2n_3)$ and $I_{\text{obs.}}(n_1n_2n_3)$ are calculated and observed total intensities of the bands with the same quantum numbers $n_1n_2n_3$

$$I(n_1n_2n_3)=\sum_{\Gamma} I(n_1n_2n_3;\Gamma). \tag{34}$$

$I_{\text{obs.}}(n_1n_2n_3)$ and $I_{\text{calc.}}(n_1n_2n_3)$ with different dipole moment models are also shown in Fig. 3. The logarithmic deviations are 0.311, 0.363, and 0.382 for DMM_1, DMM_2, and DMM_3, respectively. It is also shown that the intensity anomaly can be predicted by DMM_1, but cannot by DMM_2 and DMM_3. The ratio of $I(210)$ to $I(300)$ is 1.44 in the observation. The value is 1.09 by the first dipole moment model, while only 0.696 and 0.575 by the latter two.

From Eqs. (3)–(7), it is clearly seen that in principle DMM_1 is equivalent to DMM_2 because all the coefficients in DMM_2 are the linear combinations of those in DMM_1 by the aid of Eqs. (4)–(6). For example

$$\begin{pmatrix} C_{300}^z \\ C_{300}^y \end{pmatrix}=\begin{pmatrix} -\sqrt{3}\cos(\theta) & -2\sqrt{3}\cos(\theta) \\ -\sqrt{6}\sin(\theta)/2 & \sqrt{6}\sin(\theta)/2 \end{pmatrix}\begin{pmatrix} C_{300}^B \\ C_{030}^B \end{pmatrix}, \tag{35}$$

where θ is the angle between P–H bond and the threefold axis of the molecule in the equilibrium configuration, and $\theta=\sin^{-1}[2\sin(\phi/2)/\sqrt{3}]$ with ϕ being the H–P–H bond angle. As mentioned in Sec. III, in the practical fitting of the DMSs, the coefficients which cannot be determined well are constrained to zeros. The C_{030}^B is set to zero in DMM_1, while both C_{300}^z and C_{300}^y are fitted in DMM_2. So, practically, DMM_1 is not equivalent to DMM_2. It is easy to understand it because C_{030}^B means the third order contributions from the displacements of P–H_2 and P–H_3 to the dipole moment along P–H_1, which will be small in physical intuition. This point is also shown in Fig. 2, where the lines of u_1 varying with r_1 at different values of r_2 and r_3 are almost superposed with each other. Equation (35) shows that both C_{300}^z and C_{300}^y have the contribution from the well determined value of C_{300}^B (see Table IV), so none of them can be constrained to zero in the fitting. If the C_{030}^B is fitted in DMM_1, the result will be $C_{030}^B=-0.056\,7(58)$ Debye Å^{-3}. Only from the one standard error in the parenthesis we cannot say the value is not well determined, but it is largely correlated with C_{010}^B. The correlation coefficient[49] is -0.79 and the root mean squares of the fitting residual only decrease from 2.91×10^{-3} to 2.84×10^{-3}Debye. The fitted value of -0.0567 can be considered as ''noise'' from the *ab initio* calculation which may not be accurate enough to determine such a high order coefficient. The advantage of the DMM_1 over DMM_2 is that we can remove the noise in the first dipole moment model but cannot in the second one.

TABLE VI. Calculated intensities (in 10^{-22} cm) of $(210;A_1/lE/hE)$ bands with, only with, and without C_{120}^B term in the improved bond dipole model (DMM_1).

$(n_1n_2n_3;\Gamma)$	With C_{120}^B	Only with C_{120}^B [a]	$C_{120}^B=0$
$(210;A_1)$	3.94	1.04	0.926
$(210;lE)$	0.361	0.125	0.0601
$(210;hE)$	2.09	2.82	0.0543

[a]All other coefficients of DMM_1 in Table IV are set to zeros.

Comparing DMM_1 with the bond dipole model in Eq. (1), it can be seen that there are only C_{i00}^B terms in the latter, so DMM_1 can be called an improved bond dipole model because some inter-bond coupling terms are introduced. From the second column in Table IV, it can be seen that all the coefficients $C_{i00}^B s$ are relatively large, and the others are small except C_{120}^B. It is shown that the empirical bond dipole model is able to work well in some cases. However, it fails sometimes because of the neglecting of the relative large inter-bond coupling terms, such as the $C_{120}^B r_1(r_2^2+r_3^2)$ in PH_3 molecule. The relatively large value of C_{120}^B is assumed to be the main reason which leads to the intensity anomaly in PH_3. The contribution of C_{120}^B term to the intensities of $(210;A_1/lE/hE)$ bands is shown in Table VI. We can see from the table that the calculated intensities become much smaller if C_{120}^B is set to zero.

In Table V, we can see that DMM_3 produces the similar intensity result as that by DMM_2 except a very weak band $(110;E)$. This also can be forecasted in Table IV, where all the coefficients of DMM_2 and DMM_3 are almost the same except C_{110}^y which is only 0.0050 Debye Å^{-2} in the former while 0.0141 Debye Å^{-2} in the latter. Considering the logarithmic deviation of DMM_3 is even larger than that of DMM_2 and that R_{Eck} only rotates very small angles from R_{Prin} as mentioned in Sec. III, it is shown that the Eckart conditions

are not crucial in studying the stretching vibrational band intensities of PH_3 molecule, so we propose that it is not necessary to use the Eckart reference system in similar problems, such as the stretching in AsH_3 and SbH_3 molecules.

Although the improved bond dipole model (DMM_1) which has some physical intuition and can predict the intensity anomaly in PH_3 seems better than DMM_2 and DMM_3, there also exist large discrepancies between the calculation and the observation for some bands, such as $I(111)$ and $I(400)$. Since the experimental absolute intensity uncertainties are not so large and the band intensity is less sensitive to the force field than to the DMS,[34] it is mainly owing to two reasons in our problem, (1) the error of the *ab initio* DMS data point calculation and (2) the error from the fitting of the DMSs to the *ab initio* data. As to the first reason, the difficulty lies in the needed high accuracy of the *ab initio* calculation and the computation resources available. Some discussions about the *ab initio* dipole moment calculation can be found elsewhere.[28] Generally speaking, higher level methods with larger basis sets provide better results. But they are more expensive, especially in the multidimensional DMS cases. A compromise has to be made between the accuracy we aim at and the computation resources we can offer. At this point, we found that the DFT method with the basis set employed in this work is an economic choice for 3D stretching DMSs in PH_3 due to its moderate accuracy and time consumed. Concerning the error from the fitting of the DMSs, the problem is that it is difficult to obtain a good fitting result near the equilibrium configuration and at large coordinate displacements at the same time. The Mecke-type function has been discarded due to its poor fit in the vicinity of the equilibrium configuration which is crucial[33] to the intensity. On the contrary, the applied polynomial functions show excellent performance at small coordinate displacements, but fail to give correct asymptotic behavior. Because the wave function distribution of the excited states at large coordinate displacements increases as the vibrational quantum number increases, the correct asymptotic behavior could be more and more important for the highly excited overtones. This may be the main reason leading to the relatively large intensity discrepancy between the calculation and the observation for $(400; A_1/E)$ bands.

VI. CONCLUSION

The stretching vibrations in PH_3 molecule were studied in this work experimentally and theoretically. The band intensities and some new band centers were reported up to the third overtone based on the FTIR spectra. The 3D P–H stretching DMSs have been calculated by applying the *ab initio* DFT method. Three kinds of molecule-fixed reference systems were used for projecting the *ab initio* dipole moment vectors, and the corresponding DMSs were expanded by polynomial functions in terms of the P–H bond length displacements with molecular symmetry taken into consideration. The absolute band intensities were calculated with an ACAO Hamiltonian model and the expanded DMSs. The results agree with experimental data reasonably well. Comparison between different dipole moment models was also made. The Eckart conditions were found to be not crucial in this problem. An improved bond dipole model can predict the intensity anomaly at the second overtone by introducing some inter-bond coupling terms to the bond dipole model. Remained discrepancies between the calculation and observation were also discussed. The improved bond dipole model is readily applied to the four-dimensional stretching DMSs in SiH_4 and its isotopic species, which is being carried out by our group.

ACKNOWLEDGMENTS

This work is jointly supported by the National Natural Science Foundation of China (Grant Nos. 29903010 and 29892161) and the Foundation of Chinese Academy of Science.

[1] G. Tarrago, N. Lacome, A. Lévy, G. Guelachvili, B. Bézard, and P. Drossart, J. Mol. Spectrosc. **154**, 30 (1992).
[2] Y. T. Chen and T. Oka, J. Mol. Spectrosc. **133**, 148 (1989); D. Papoušek, H. Birk, U. Magg, and H. Jones, *ibid.* **135**, 105 (1989).
[3] A. Ainetschian, U. Häring, G. Spiegl, and W. A. Kreiner, J. Mol. Spectrosc. **181**, 99 (1996).
[4] X. J. Wang, M. Sci. thesis, Dalian Institute of Chemical Physics, Dalian, China, 1991.
[5] P. Drossart, E. Lellouch, B. Bézard, J. P. Maillard, and G. Tarrago, Icarus **83**, 248 (1990).
[6] K. S. Noll and H. P. Larson, Icarus **89**, 168 (1990).
[7] P. Drossart, B. Bézard, J. P. Maillard, G. Tarrago, N. Lacome, G. Poussigue, A. Lévy, and G. Guelachvili, Bull. Am. Astron. Soc. **19**, 848 (1987).
[8] M. S. Child and L. Halonen, Adv. Chem. Phys. **57**, 1 (1984).
[9] D. C. McKean and P. N. Schatz, J. Chem. Phys. **24**, 316 (1956).
[10] A. Baldacci, V. M. Devi, and K. N. Rao, J. Mol. Spectrosc. **81**, 179 (1980).
[11] H. Hollenstein, R. R. Marquardt, M. Quack, and M. A. Suhm, J. Chem. Phys. **101**, 3588 (1994); R. Signorell, R. R. Marquardt, M. Quack, and M. A. Suhm, Mol. Phys. **89**, 297 (1996).
[12] H.-R. Dübal, T.-K. Ha, M. Lewerenz, and M. Quack, J. Chem. Phys. **91**, 6698 (1989); T.-K. Ha, M. Lewerenz, R. R. Marquardt, and M. Quack, *ibid.* **93**, 7097 (1990).
[13] E. Kauppi and L. Halonen, J. Chem. Phys. **90**, 6980 (1989); **92**, 3278 (1990); E. Kauppi, J. Mol. Spectrosc. **167**, 314 (1994).
[14] I. Schek, J. Jortner, and M. L. Sage, Chem. Phys. Lett. **64**, 209 (1979); L. Halonen, J. Mol. Spectrosc. **120**, 175 (1986).
[15] L. Halonen and M. S. Child, Mol. Phys. **46**, 239 (1982).
[16] R. Mecke, Z. Elektrochem. **54**, 38 (1950).
[17] H. Lin, L. F. Yuan, and Q. S. Zhu, Chem. Phys. Lett. **308**, 137 (1999).
[18] H. Lin, L. F. Yuan, D. Wang, and Q. S. Zhu, Chin. Phys. Lett. **17**, 13 (2000).
[19] M. Lewerenz and M. Quack, Chem. Phys. Lett. **123**, 197 (1986).
[20] J. L. Liao and Q. S. Zhu, J. Mol. Spectrosc. **183**, 414 (1997).
[21] D. C. McKean, A. R. Morrison, and M. I. Kelly, Chem. Phys. Lett. **109**, 347 (1984); A. Campargue, F. Stoeckel, and M. C. Terrile, Chem. Phys. **110**, 145 (1986).
[22] B. R. Henry, A. W. Tarr, O. S. Mortensen, W. F. Murphy, and D. A. C. Compton, J. Chem. Phys. **79**, 2583 (1983).
[23] H. G. Kjaergaard, H. Yu, B. J. Schattka, B. R. Henry, and A. W. Tarr, J. Chem. Phys. **93**, 6239 (1990).
[24] H. G. Kjaergaard, B. R. Henry, and A. W. Tarr, J. Chem. Phys. **94**, 5844 (1991).
[25] H. G. Kjaergaard, G. D. Goddard, and B. R. Henry, J. Chem. Phys. **95**, 5556 (1991).
[26] H. G. Kjaergaard and B. R. Henry, J. Chem. Phys. **96**, 4841 (1992).
[27] H. G. Kjaergaard, D. M. Turnbull, and B. R. Henry, J. Chem. Phys. **99**, 9438 (1993); H. G. Kjaergaard, B. R. Henry, H. Wei, S. Lefebvre, Jr., T. Carrington, O. S. Mortensen, and M. L. Sage, *ibid.* **100**, 6228 (1994); H. G. Kjaergaard and B. R. Henry, Mol. Phys. **83**, 1099 (1994).
[28] H. G. Kjaergaard, C. D. Daub, and B. R. Henry, Mol. Phys. **90**, 201 (1997); H. G. Kjaergaard, K. J. Bezar, and K. A. Brooking, *ibid.* **96**, 1125 (1999).

[29] H. G. Kjaergaard, Z. M. Rong, A. J. McAlees, D. L. Howard, and B. R. Henry, J. Phys. Chem. A **104**, 6398 (2000).
[30] J. R. Fair, O. Votava, and D. J. Nesbitt, J. Chem. Phys. **108**, 72 (1998).
[31] O. L. Polyansky, P. Jensen, and J. Tennyson, J. Chem. Phys. **105**, 6490 (1996).
[32] W. Gabriel, E.-A. Reinsch, P. Rosmus, S. Carter, and N. C. Handy, J. Chem. Phys. **99**, 897 (1993).
[33] H. Lin, L. F. Yuan, S. G. He, X. G. Wang, and Q. S. Zhu, J. Chem. Phys. **112**, 7484 (2000).
[34] S. G. He, L. F. Yuan, H. Lin, Q. S. Zhu, and X. G. Wang, J. Phys. Chem. A (to be published).
[35] C. Eckart, Phys. Rev. **47**, 552 (1935); P. Pulay, G. Fogarasi, F. Pang, and J. E. Boggs, J. Am. Chem. Soc. **101**, 2550 (1979).
[36] P. R. Bunker, *Molecular Symmetry and Spectroscopy* (Academic, New York, 1979).
[37] L. S. Rothman, C. P. Rinsland, A. Goldman *et al.*, J. Quant. Spectrosc. Radiat. Transf. **60**, 665 (1998).
[38] A. D. Becke, J. Chem. Phys. **98**, 5648 (1993); C. Lee, W. Yang, and K. G. Parr, Phys. Rev. B **37**, 785 (1988).
[39] K. Raghavachari and G. W. Trucks, J. Chem. Phys. **91**, 1062 (1989), and references therein.
[40] GAUSSIAN 94, Revision B.1, M. J. Frisch, G. W. Trucks, H. B. Schlegel *et al.*, Gaussian, Inc., Pittsburgh, PA, 1995.
[41] C. R. Le Sueur, S. Miller, J. Tennyson, and B. T. Sutcliffe, Mol. Phys. **76**, 1147 (1992).
[42] W. H. Press, S. A. Teukolsky, W. T. Vetterling, and B. P. Flannery, *Numerical Recipes in C, The Art of Scientific Computing* (Cambridge University Press, New York, 1992).
[43] J. S. Griffith, *The Theory of Transition-Metal Ions* (Cambridge University Press, Cambridge, 1961).
[44] L. Halonen, J. Chem. Phys. **106**, 831 (1997).
[45] D. Papoušek and K. Sarka, J. Mol. Spectrosc. **28**, 125 (1968).
[46] L. Halonen, M. S. Child, and S. Carter, Mol. Phys. **47**, 1097 (1982); L. Halonen and M. S. Child, Comput. Phys. Commun. **51**, 173 (1988).
[47] L. Halonen, J. Mol. Spectrosc. **120**, 175 (1986).
[48] D. Wang, Q. Shi, and Q. S. Zhu, J. Chem. Phys. **112**, 9624 (2000).
[49] R. M. Lees, J. Mol. Spectrosc. **33**, 124 (1970).
[50] T. Tipton, J. I. Choe, and S. G. Kukolich, J. Phys. Chem. **90**, 1534 (1986).
[51] A. G. Maki, R. L. Sams, and W. B. Olson, J. Chem. Phys. **58**, 4502 (1973).
[52] K. Kijima and T. Tanaka, J. Mol. Spectrosc. **89**, 62 (1981).
[53] D. A. Helms and W. Gordy, J. Mol. Spectrosc. **66**, 206 (1977).
[54] P. B. Davies, R. M. Neumann, S. C. Wofsy, and W. Klemperer, J. Chem. Phys. **55**, 3564 (1971).